Unveiling the magmatic plumbing system of Tatun volcano in northern Taiwan using joint inversion of local and teleseismic P-wave data

Hsin-Hua Huang[1,1], E.-S Wu[2,2], C.-H Lin[1,1], Y.-T Ko[2,2], M.-H Shih[1,1], and I Koulakov[3,3]

[1]Academia Sinica
[2]National Taiwan University
[3]Trofimuk Institute of Petroleum Geology and Geophysics SB RAS

November 30, 2022

Abstract

The Tatun volcano group (TVG) proximate to the 7-million-population metropolis Taipei has long been a central concern in volcanic hazard in the Taiwan. While the TVG has been previously considered an extinct volcano, recent evidences suggested a much younger age of the last eruption event (˜6000 years) and the possible existence of magma reservoir beneath the TVG. To examine and unveil the TVG magmatic plumbing system in detail, the local P-wave travel time data and the teleseismic waveform data from a new island-wide Formosa Array Project are combined for a 3D joint inversion. The new model reveals a pronounced magma reservoir with high fraction of melt (˜16.5%) beneath the TVG at 5-25 km and better illuminate the deep magmatic structures that may suggest delamination processes in the northern Taiwan. Plain Language Summary The Tatun volcano group (TVG) is close to the metropolis Taipei and poses a direct threat to the 7 million population nearby. While the TVG was thought to be extinct in the past, recent studies found much younger eruption records (˜6000 years) and some indications of alive magma chamber underneath. To better understand whether the magma chamber exists and what its geometry is, the Formosa Array project deployed 120 broadband stations in the northern Taiwan well covering the TVG area. Integrating the Formosa Array dataset, a new 3-D P-wave velocity model is constructed and shows a clear image of the magma chamber beneath the TVG at the depth of 5-25 km. Deep magmatic structures are also imaged and suggest the crust in the northern Taiwan was thickened and has possibly peeled off during the mountain building processes.

Unveiling the magmatic plumbing system of Tatun volcano in northern Taiwan using joint inversion of local and teleseismic P-wave data

H.-H. Huang[1], E.-S. Wu[2], C.-H. Lin[1], J. Y.-T. Ko[2], M.-H. Shih[1], and I. Koulakov [3,4,5]

[1] Institute of Earth Sciences, Academia Sinica, Taipei, Taiwan.

[2] Institute of Oceanography, National Taiwan University, Taiwan.

[3] Trofimuk Institute of Petroleum Geology and Geophysics SB RAS, Novosibirsk, Russia.

[4] Novosibirsk State University, Novosibirsk, Russia.

[5] Institute of Volcanology and Seismology FEB RAS, Petropavlovsk-Kamchatsky, Russia

Corresponding author: Hsin-Hua Huang (hhhuang@earth.sinica.edu.tw)

Key Points:

- A pronounced low velocity anomaly (>15%) beneath the Tatun volcano group is found at the depths of 5-25 km as the magma reservoir.
- A high melt fraction of ~16% for the magma reservoir is estimated.
- The new model better illuminates the deep magmatic structures and suggests delamination processes in the northern Taiwan.

Abstract

The Tatun volcano group (TVG) proximate to the 7-million-population metropolis Taipei has long been a central concern in volcanic hazard in the Taiwan. While the TVG has been previously considered an extinct volcano, recent evidences suggested a much younger age of the last eruption event (~6000 years) and the possible existence of magma reservoir beneath the TVG. To examine and unveil the TVG magmatic plumbing system in detail, the local P-wave travel time data and the teleseismic waveform data from a new island-wide Formosa Array Project are combined for a 3D joint inversion. The new model reveals a pronounced magma reservoir with high fraction of melt (~16.5%) beneath the TVG at 5-25 km and better illuminate the deep magmatic structures that may suggest delamination processes in the northern Taiwan.

Plain Language Summary

The Tatun volcano group (TVG) is close to the metropolis Taipei and poses a direct threat to the 7 million population nearby. While the TVG was thought to be extinct in the past, recent studies found much younger eruption records (~6000 years) and some indications of alive magma chamber underneath. To better understand whether the magma chamber exists and what its geometry is, the Formosa Array project deployed 120 broadband stations in the northern Taiwan well covering the TVG area. Integrating the Formosa Array dataset, a new 3-D P-wave velocity model is constructed and shows a clear image of the magma chamber beneath the TVG at the depth of 5-25 km. Deep magmatic structures are also imaged and suggest the crust in the northern Taiwan was thickened and has possibly peeled off during the mountain building processes.

1 Introduction

The Taiwan orogenic belt is the product of oblique collision between the Eurasian plate (EP) and the Philippine Sea plate (PSP), where the EP subducts eastward at the Manila trench to the south and the PSP subducts northward at the Ryukyu trench to the east (Figure 1a). The collision initiated 4-6 Ma as the PSP Luzon arc collides toward the EP continental margin and propagated southward from the northern Taiwan (Suppe, 1984; Liu et al., 2001). The northern Taiwan has therefore experienced a tectonic transition from collision to post-collisional extension since ca. 2.8 Ma (Teng, 1996; Wang et al., 2004), producing multiple-stage and complex volcanisms (Figure 1a). In the east offshore, the PSP subduction and subsequent back-arc opening created the Ryukyu volcanic arc and a series of submarine volcanoes in the Okinawa trough. In the north offshore, the northern Taiwan volcanic zone (NTVZ) in NE-SW trending was suggested to form by the extensional collapse of the mountain belt (Wang et al., 1999; 2004). The most obvious inland manifestation of this NTVZ is the Tatun volcano group (TVG) located in the north of Taipei. Its proximity within 15 km to the metropolis Taipei where more than 7 million population resides and to two nuclear power plants on the northern coast has posed a sever threat to the society of Taiwan (Konstantinou et al., 2007).

The TVG has been considered as an extinct volcano until recently since no volcanic eruption was recorded in historical times (Kim, 2005; Konstantinou et al., 2007). The two major time periods of volcanism pulses were suggested at 2.8-2.5 Ma and 0.8-0.2 Ma by the radiometric dating of volcanic rocks (Tsao, 1994; Wang and Chen, 1990; Song et al., 2000).

However, recent studies by analyzing the characters of volcanic ash in the northern Taipei basin and volcaniclastic deposits in the TVG found much younger eruption records that are 20 Ka and 6000 years ago (Chen and Lin, 2002; Belousov et al., 2010). Meanwhile, growing evidences also suggested a magma reservoir likely existing beneath the TVG. For instance, the high 3He/4He ratio from the fumarolic and bubbling gasses of TVG hot springs requires a deep magmatic origin, i.e. magma reservoir (Yang et al., 1999; Lee et al., 2008). The seismic observations of S-wave shadows and P-wave delays from a deep subduction earthquake suggested the rough location of a magma reservoir at around 30-km depth slightly to the east of the TVG (Lin, 2016). In combination with the vigor of hydrothermal activity and miscroseismicity at several fumarole sites (Lin et al., 2005; Konstantinou et al., 2007; Lin, 2017a, b), all these observations indicate that the TVG is possibly still active. However, the detailed geometry of its magmatic plumbing system remains poorly understood.

To illuminate the magmatic plumbing structure of the TVG, a deployment of dense broadband seismic array, named Formosa Array (Academia Sinica, Institute of Earth Sciences, 2017), was launched in 2017 and has installed 120 out of 140 planned stations by October 2019 (Figure 1b, blue squares). The station spacing is ~5 m uniformly across plain and mountain areas, providing a new opportunity to improve tomographic imaging of the northern Taiwan (Wu et al., 2007; Kuo-Chen et al., 2012; Huang et al., 2014a, b). In this study, we combine the teleseismic waveform data from the Formosa Array and the local P-wave picking data from an integrated seismic network to conduct a 3D joint inversion (Figure 1c and 1d). Benefiting from the uniform and dense station distribution of the Formosa Array, the joint inversion improves the resolution around the northern coast (north of latitude 25.0°) that well covers the TVG area. The new model reveals a pronounced low velocity anomaly (>15%) beneath the TVG at 5-25 km as likely the magma reservoir. Through calculation, this reservoir contains a high fraction of andesitic melt to be ~16.5%. A deeper partial melting feature (~2.2% basaltic melt) originating at the depth around 50 km with no clear connection to the subduction zone indicates a delamination-origin rather than subduction-origin plumbing system, consistent with the magmatism signature of the NTVZ. These findings unveil an active plumbing system beneath the TVG and therefore continuing monitoring the TVG activity is more important than ever.

2 Data and Methods

2.1 Seismic networks and data

We use both local earthquake and teleseismic data for a joint inversion in this study. The local earthquake data are compiled from an integrated regional seismic network that combines (1) the Central Weather Bureau permanent seismic network (CWBSN) (Shin 1992), (2) Taiwan Strong Motion Instrumentation Program (TSMIP) (Shin et al., 2003), (3) Broadband Array in Taiwan for Seismology (BATS) (Kao et al., 1998), (4) Data-exchanging seismic stations of Japan Meteorological Agency (JMA) at the western Ryukyu arc (Wu et al., 2009), and (5) part stations of TAIGER project including inland broadband stations and western offshore OBS arrays (Kuo-Chen et al., 2012). A total of 671 stations are used in the study area (Figure 1b, purple squares). Based on the data criteria that (1) each event at least recorded by 4 stations, (2) gap angle less than 180°, (3) focal depth shallower than 120 km, and (4) picking quality less than

level 2 (level 0–4 in total and 0 is the best, referring to the CWB picking criteria), 60,081 events are sorted out from 1991 to 2017. To avoid the dominance from compactly-distributed earthquake clusters for better conditioning the inversion, a 3-D event grouping method (Liang et al, 2004; Huang et al., 2014a) with 2 km radius is applied to homogenize the event distribution and reduce the event number to 3,587 in the end (Figure 1b).

For the teleseismic data, we collect the waveform data of 371 teleseismic events (ML≥5.0) in a distance range of 30°-90° recorded by the newly-deployed Formosa Array (Academia Sinica, Institute of Earth Sciences, 2017) from April 2018 to October 2019 (Figure 1c, gray dots). The vertical component of waveform data is bandpass-filtered in 0.08-0.15 Hz to measure the P-wave relative travel times between stations using the adaptive stacking method (Rawlinson and Kennett, 2004). Through the iterative measuring process, only those signal-to-noise ratio (S/N) larger than 5 and the cross-correlation coefficient (CC) greater than 0.9 are retained. After final visual screening, we obtain a total of 148 events in the end (Figure 1c, red dots). Figure S1 shows the measured relative P-wave travel times for four representative events coming from different quadrants. The travel times for the stations around the TVG are consistently delayed regardless of the event azimuth, implying the existence of low velocity anomalies underneath.

2.2 Joint inversion

A recently developed tomographic code for multi-dataset joint inversion is employed in this study (Huang et al., 2014a,b; Huang et al., 2015), in which the absolute travel-time residuals from local earthquake data and the relative travel-time residuals from teleseismic data are simultaneously minimized (Text S1). For travel-time calculation, the 3-D spherical pseudo-bending method (Um and Shearer, 1987; Koketsu and Sekine, 1998) is used to trace and update both local earthquake and teleseismic ray paths at each iteration for a nonlinear approximation. The model grids are parameterized with 4 km in longitude and latitude and increasing intervals from -5 to 120 km in depth as shown in Table S1. The 3-D P-wave velocity (VP) model of Huang et al. (2014a) is interpolated to the current model grids and used as the initial model for joint inversion. The damping and smoothing factors are chosen to be 30 and 10 after a series of trade-off tests (Text S1 and Figure S2).

We iterate the inversion until the root-mean-square of travel-time residuals (RMS) reduces insignificantly. After 4 iterations, the RMS is reduced from 0.227 to 0.124 s, a 45% reduction. The residual distribution for local earthquake and teleseismic data is plot separately in Figure S3. Both the residuals are effectively reduced and concentrated toward the zero after the inversion.

3 Model resolution and Results

3.1 Checkerboard tests and resolvability index

The checkerboard test is conducted for assessing general resolution power of the obtained velocity model (details please refer to Text S3). In Figure S4, the results of the checkerboard tests show good recovery in most inland region and to the east of longitude 122.1° above the depth of 30 km. Below 30 km, the well-recovered region is gradually shifted eastward as the depth increases. To the depth of 90 km, the well-recovered region is primarily limited beneath

the Ilan plan and its east offshore. The recovered checkerboard model is then used to calculate a resolvability index, R, at each model node (Equation S1). R ranges from 0 to 1 where the value 1, 0.5, and 0 indicate the node is 100%, 0%, and −100% recovered, respectively. R = 0.6 is used as a lower bound for the resolvable nodes in tomographic images (Huang et al., 2015).

3.2 Model results and comparison

The model slices at different depths with and without Formosa Array teleseismic data are shown in Figure 2, where poorly resolved areas are defined as R < 0.6 and masked. In comparison with the inversion using local earthquake data only, joint inversion integrating teleseismic data greatly improves the resolution north of latitude 25.0°, especially at depths of 10-40 km. Corresponding checkerboard test results are shown in Figure S4. With this resolution improvement, a pronounced low velocity anomaly (LVA) stands out beneath the Tatun volcano group (TVG) at the depth slice of 12 km (Figure 2b, L1). This LVA is vertically elongated at a depth range of 5-25 km as shown in cross-sections of Figure 3b and 3c. In the NW-SE cross-section CC', another LVA (L2) appears at the depths of 30-40 km and tilts southeastwardly. The shallow LVAs L3 represent the sedimentary rocks of Linkou tableland that possibly smear a bit downward in depth. Movie S1 displays a rotational view for better illustrating the 3-D geometry of the LVAs.

At a regional scale, the cross-sections of Figure 3d-f show the deep structures beneath the northern Taiwan. The LVA L5 at deep depth around 70 km indicates the partial melting (Lin et al., 2004; Huang et al., 2014a), originating from the subducting PSP characterized by the high velocity anomaly (HVA), H3. The shallow HVA H4 and LVA L6 together represent the thicken crust of the orogenic belt down to ~55-km depth, where the H4 represents faster metamorphic rocks of exhumed Central Range relative to the slow sedimentary rocks in the western foothill and plain (e.g. L3) and the L6 represents slower mid-to-lower crustal accretionary wedge relative to fast oceanic crust and mantle to the east (Figure 2c and 2d). The LVA L7 in Figure 2a and 3d marks the Ilan plain basin structure (Huang et al., 2012). The H2, on the other hand, denotes one of the several anomalous high velocity blobs at mid-crustal depths in the region (e.g. Figure 2c and 3e), which will be discussed in later sections. Movie S2 and S3 provide the E-W and N-S cross-sectional views for 3-D spatial distribution of the velocity anomalies.

3.2 Characteristic-model test

Characteristic-model tests are further conducted to evaluate the new findings of TVG-related LVAs, i.e. L1 and L2 (Figure 2, 3b, and 3c). We input two synthetic LVAs according to the geometry of L1 and L2 in different scenarios, such as connected vs. not connected, and L1 alone vs. both existed (Figure S5). Detailed descriptions are referred to Text S3. Based on the recovery results, L2 is more likely a separate anomaly rather than the consequence of smearing effect from L1. Adding random noise with 0.12-s standard deviation (based on the residual RMS of actual inversion) to the synthetic data provides little effect on the results (Figure S6). The L2 is in a conduit shape tilting to the southeast and roughly terminates at the depth of 45 km (Figure 3d). We also note that using different initial model (e.g. 1-D velocity model) will not change the tomographic imaging much (Figure S7).

4 Discussion and Conclusions

The new model derived from the joint inversion with both local earthquake and teleseismic data unveils the geometry and extent of the TVG magma reservoir (Figure 3b and 3c). The magma reservoir is ~10 km in diameter and at the depths of 5-25 km in a vertically elongated shape, shallower than the previously proposed depth of ~30 km (Lin, 2016). The geometry of the imaged reservoir is proved to be robust through both checkerboard and characteristic-model tests (Figure S4-S7). More importantly, its magnitude of P-wave velocity (Vp) reduction is close to -15%. Since the regularization often damps the magnitude of velocity perturbations in the inversion, we conduct another characteristic-model test with different input Vp reductions for the reservoir to assess the actual velocity anomaly magnitude (Text S3 and Figure S8). The results find that a greater Vp reduction of -16% is needed to fit the inversion results (Figure S5a, 5d, and 5g), a large number comparable to recently reported high-melt-reservoirs at Long Valley caldera in U.S.A. (Flinders et al., 2018) and Santorini volcano in Greece (McVey et al., 2019).

To further estimate the melt fraction, we use Gassmann's relations which are valid for equilibrated pore pressures with no assumptions on pore geometries (Chu et al., 2010; Huang et al., 2015). The calculation and used parameters are described in Text S4 and Table S2 in detail. Assuming andesitic melt and granite frame rock with 16% Vp reduction, a high melt fraction of ~16.5% is estimated (Figure S9a). For volume estimation, since a number of factors such as temperature, composition, and tomographic resolution prevent the weaker anomalies from being robustly interpreted as melt, a conservative choice of 5% Vp reduction is used and results in a reservoir volume of 3,056 km3 and a melt volume of 504 km3, respectively (Text S4). Although the uncertainty of this simplified estimation is not negligible, the high melt fraction of 16.5% is prone to be reasonable considering the recent observations of S-wave shadow from a deep subduction event (Lin, 2016)—A phenomena that S-wave energy is nearly depleted when propagating across a fluid-rich reservoir (Einarsson, 1978). Nevertheless, further studies will be needed to clarify whether this shadow is caused by the strong attenuation or geometrical diffraction of the high melt fraction in the Tatun magma reservoir.

The L2 structure is another intriguing finding in the new model, with a conduit-like geometry tilting to the southeast (Figure 3c and 3d). Its magnitude of Vp reduction is about -8% and the actual magnitude is estimated to be -13% through synthetic tests (Text S3 and Figure S7). This -13% is not able to account for by only temperature or composition variations (Huang et al., 2015). Considering that the Moho depth in this region is around 25-30 km from previous studies (Kim et al., 2004; Wang et al., 2010; Ustaszewski et al., 2012), the L2 is mostly below the Moho and likely represents the partial melting in the upper mantle. By attributing a basaltic magmatic origin to it and taking the same -5% Vp reduction for volume calculation, we obtain a melt fraction of ~2.2% with a relatively small melt volume of 25 km3 (Text S4 and Figure S9b).

In a regional magmatism context, this L2 partial melting could originate from the PSP subduction, such as L5 in Figure 3d (Teng, 1996); or from the post-collisional delamination processes (Wang et al., 1999, 2004). In the subduction scenario, ascending melt/fluid pathways from near the subducting slab edge to the Kuishantao Island has been proposed by tracking high Vp/Vs anomalies (Lin et al., 2004). This can be roughly seen in our Figure 3f, where the L5 rising toward the L4 at the depths of 20-40 km and then the L4 laterally links to the Kuishantao Island magma reservoir, L8. This pathway is, however, debated since the low Vp of L4 was instead interpreted as serpentinized wedge in other studies (Chou et al., 2009; Huang et al.,

2014a). How the ascending melt from L5 passes through and interacts with the L4 is still unclear. For the L2 that seems to bottom at 45-50 km, no identifiable pathways from L5 to L2 are observed in the model (Figure 3d), Furthermore, the existence and possible tear of vertically bended Eurasian plate in this region (Teng, 2000; Lallemand et al., 2001; Ustaszewski et al., 2012; Huang et al., 2014b) also complicates (hinders) the way the melt rising westward to the TVG.

Alternatively, a more straightforward and perhaps more plausible scenario for explaining the L2 melting feature is the local delamination processes, a tectonic process that has been reported in many places undergoing post-orogenic extensional environments (Kay and Kay, 1993; Leech, 2001; Fillerup et al., 2010; Gogus et al., 2017). Stress state, GPS, and geotectonics all indicate that the northern Taiwan is now experiencing the extensional collapsing of the mountain belt (Teng, 1996; Ching et al., 2011; Huang et al., 2012). Analyses of NTVZ magmatism in spinel facies showed mantle source signatures and suggested delamination-induced partial melting originating within depths no greater than 70 km (Wang et al., 1999, 2004; Chung et al., 2001). Such scenario is consistent with several observations in our model. First, the L2 anomaly terminates abruptly around 45-50 km (< 70 km), with no clear connection to the subduction partial melting, L5 (Figure 3d). Second, a dipping high velocity anomaly (H1) at >30-km depth roughly in parallel with the L2 likely represent a partial delaminating (peeling-off) crustal/subcrustal fragment which had been thickened and eclogized (Figure 3b and 4a). This localized delamination process then allows the upwelling of the asthenosphere to form partial melting, L2 (Figure 3c and 4b). Furthermore, in Figure 3e, a clear transition can be seen from intact and thickened crust at cross-section distances 0-80 km to the crust with sporadic high/low velocity anomalies at distances greater than 80 km. This transition implies that the northern part of the crust (>80 km) may have been perturbed by distributed high-velocity magmatic underplating (e.g. H2) due to delamination-induced magmatism activity in the past (Figure 4b). We therefore speculate a delamination origin of Tatun volcano plumbing system.

The 120 uniformly-distributed broadband stations of Formosa Array provide unique opportunity to illuminate the Tatun volcanic plumbing system and deep subsurface velocity structure beneath the northern Taiwan in greater detail (Figure 1a). The wealth of this new dataset will facilitate further studies and findings to come. The unveiled Tatun magma reservoir shows high melt content (~16.5%) and shallower location (top at 5-km depth) than previously thought. While these characteristics do not imply an imminent eruption, they are clear indications that the Tatun volcano is an active volcano with potentially ~504 km3 melt in storage. Monitoring all kinds of activity in the TVG (e.g. hydrothermal, microseismicity, gass/fluid chemistry, CO2/SiO2 flux, ground deformation, etc.) as now the Tatun volcano observatory operates is therefore of great importance for volcanic hazard forecasting and mitigation..

Acknowledgments, Samples, and Data

We thank Kuo-Lung Wang for valuable discussion. The data are available on request to the Central Weather Bureau (https://www.cwb.gov.tw/V8/C/E/index.html) and the Formosa Array (https://fmarray.earth.sinica.edu.tw/). This work was supported by Ministry of Science and Technology, Grants 107-2923-M-001-006-MY3, 108-2116-M-001-009, and 108-2119-M-001-

010, and Russian Foundation for Basic Research, Grant 18-55-52003_MNT_a.The text ends with an acknowledgment section and statement that includes:

References

Aki, K., A. Christoffersson, & Husebye, E. S. (1977), Determination of the three-dimensional seismic structure of the lithosphere. *J. Geophys. Res.*, 82, 277–296. doi:10.1029/JB082i002p00277.

Belousov, A., Belousova, M., Chen, C.H., & Zellmer, G.F. (2010), Deposits, character and timing of recent eruptions and gravitational collapses in Tatun Volcanic Group, Northern Taiwan: hazard-related issues. *J. Volcanol. Geotherm. Res.*, 191, 205–221.

Chen, C.-H., & Lin, S.-B. (2002), Eruptions younger than 20 ka of the Tatun Volcano Group as viewed from the sediments of the Sungshan Formation in Taipei Basin. *West Pacific Earth Science*, 2, 191–204.

Ching, K.-E., Hsieh, M.-L., Johnson, K. M., Chen, K.-H., Rau, R.-J., & Yang, M. (2011), Modern vertical deformation rates and mountain building in Taiwan from precise leveling and continuous GPS observations, 2000–2008. *J. Geophys. Res.*, 116, B08406, doi:10.1029/2011JB008242.

Chou, H.-C., Kuo, B.-Y., Chiao, L.-Y., Zhao, D., & Hung, S.-H. (2009), Tomography of the westernmost Ryukyu subduction zone and the serpentinization of the fore-arc mantle. *J. Geophys. Res.*, 114, B12301. doi:10.1029/2008JB006192.

Chu, R., Helmberger, D. V., Sun, D., Jackson, J. M., & Zhu, L. (2010), Mushy magma beneath Yellowstone. *Geophys. Res. Lett.*. 37, L01306. doi:10.1029/2009GL041656

Chung, S. L., Wang, K. L., Crawford, A. J., Kamenetsky, V. S., Chen, C.-H., Lan, C. Y., & Chen, C. H. (2001), High-Mg potassic rocks from Taiwan: implication for the genesis of orogenic potassic magmas. *Lithos*, 59, 153-170.

Crotwell, H. P., Owens, T. J., & Ritsema, J. (1999), The TauP toolkit: Flexible seismic travel-time and ray-path utilities. *Seismol. Res. Lett.*, 70(2), 154–160.

Einarsson, P. (1978), S-wave Shadows in the Krafla Caldera in NE-Iceland, Evidence for a Magma Chamber in the Crust. *Bull. Volcanol.*, 41-3, 187-195.

Fillerup, M. A., Knapp, J. H., Knapp, C. C., & Raileanu, V. (2010), Mantle earthquakes in the absence of subduction? Continental delamination in the Romanian Carpathians: Lithosphere, v. 2, p. 333–340, doi:10.1130/L102.1.

Flinders, A., Shelly, D. R., Dawson, P. B., Hill, D. P., Tripoli, B., & Shen, Y. (2018), Seismic evidence for signigicant melt beneath the Long Valley Caldera, California. *Geology*, 46 (9),799–802.

Gassmann, F. (1951), Elastic waves through a packing of spheres. *Geophysics*, 16(4), 673–685. https://doi.org/10.1190/1.1437718.

Göğüş, O. H., Pysklywec, R. N., Şengör, A. M. C., & Gün, E. (2017). Drip tectonics and the enigmatic uplift of the Central Anatolian Plateau. *Nature Communications*, 8, 1538. https://doi.org/10.1038/s41467-017-01611-3.

Huang, H.-H., Shyu, J. B. H., Wu, Y.-M., Chang, C.-H., & Chen, Y.-G. (2012), Seismotectonics of northeastern Taiwan: Structural characteristics of a transitional area from wanning collision to subduction and post-collisional extension. *J. Geophys. Res.*, 117, B01313. doi:10.1029/2011JB008852.

Huang, H.-H., Xu, Z., Wu, Y.-M., Song, X., Huang, B.-S., & Minh, N. L. (2013), First Local Seismic Tomography for Red River Shear Zone, northern Vietnam: Stepwise inversion employing crustal P and Pn waves. *Tectonophysics*, 584, 230-239.

Huang, H.-H., Wu, Y.-M., Song, X., Chang, C.-H., Lee, S.-J., Chang, T.-M., & Hsieh, H.-H. (2014), Joint Vp and Vs tomography of Taiwan: Implications for subduction-collision orogeny. *Earth Planet. Sci. Lett.*, 392, 177-191.

Huang, H.-H., Wu, Y.-M., Song, X., Chang, C.-H., Kuo-Chen, H., & Lee, S.-J. (2014), Investigating the lithospheric structures beneath Taiwan region by nonlinear joint inversion of local and teleseismic P-wave data: Slab continuity and deflection. *Geophys. Res. Lett.*, 41, doi:10.1002/2014GL061115.

Huang, H.-H., Lin, F.-C., Schmandt, B., Farrell, J., Smith, R. B., & Tsai, V. C. (2015), The Yellowstone magmatic system from the mantle plume to the upper crust. *Science*, 348. doi:10.1126/science.aaa5648.

Kao, H., Jian, P. R., Ma, K. F., Huang, B. S., & Liu, C. C. (1998), Moment-tensor inversion for offshore earthquakes east of Taiwan and their implications to regional collision. *Geophys. Res. Lett.*, 25(19), 3619–3622.

Kay, R.W., & Kay, S.M. (1993), Delamination and Delamination Magmatism. *Tectonophysics*, 219, 177–189. doi:10.1016/0040-1951(93)90295-U.

Kennett, B. L. N., Engdahl, E. R., & Buland, R. (1995), Constraints on seismic velocities in the Earth fromtravel times. *Geophys. J. Int.*, 122, 108–112.

Kim, K. H., Chiu, J.-M., Kao, H., Liu, Q., & Yeh, Y.-H. (2004), A preliminary study of crustal structure in Taiwan region using receiver function analysis. *Geophys. J. Int.*, 159, 146–164.

Kim, K. H., Chang, C.-H., Ma, K.-F., Chiu, J.-M., & Chen, K.-C. (2005), Modern seismic observations in the Tatun volcano region of northern Taiwan: seismic/volcanic hazard adjacent to the Taipei metropolitan area. *Terr. Atm. Ocean. Sci.*, 16, 579–594.

Koketsu, K., & Sekine, S. (1998), Pseudo-bending method for three-dimensional seismic ray tracing in a spherical earth with discontinuities. *Geophys. J. Int.*, 132(2), 339–346.

Konstantinou, K. I., Lin, C.-H., & Liang, W.-T. (2007), Seismicity characteristics of a potentially active Quaternary volcano: the Tatun Volcano group, northern Taiwan. *J. Volcanol. Geotherm. Res.*, 160. doi:10.1016/j.jvolgeores.2006.09.009.

Kuo-Chen, H., Wu, F. T., & Roecker, S. W. (2012), Three-dimensional P velocity structures of the lithosphere beneath Taiwan from the analysis of TAIGER and related seismic datasets. *J. Geophys. Res.*, 117, B06306, http://dx.doi.org/10.1029/2011JB009108.

Lallemand, S., Font, Y., Bijwaard, H., & Kao, H. (2001), New insights on 3-D plates interaction near Taiwan from tomography and tectonic implications. *Tectonophysics*, 335, 229–253.

Lee, H.F., Yang, T.F., Lan, T.F., Chen, C.H., Song, S.R., & Tsao, S. (2008), Temporal variations in gas compositions of fumaroles in the Tatun Volcano Group, northern Taiwan. *J. Volcanol. Geotherm. Res.*, 178. doi:10.1016/j.jvolgeores.2008.06.005.

Leech, M. L. (2001), Arrested orogenic development: eclogitization, delamination, and tectonic collapse. *Earth and Planet. Sci. Lett.*, 185, 149–159. doi:10.1016/S0012-821X(00)00374-5.

Liang, C., Song, X., & Huang, J. (2004), Tomographic inversion of Pn travel times in China. *J. Geophys. Res.*, 109, B11304, http://dx.doi.org/10.1029/2003JB002789.

Lin, J.-Y., Hsu, S.-K., & Sibuet, J.-C. (2004), Melting features along the western Ryukyu slab edge (northeast Taiwan): Tomographic evidence. *J. Geophys. Res.*, 109, B12402. doi:10.1029/2004JB003260.

Lin, C.H., Konstantinou, K.I., Liang, W.T., Pu, H.C., Lin, Y.M., You, S.H., & Huang, Y.P. (2005), Preliminary analysis of volcanoseismic signals recorded at the Tatun volcano group, northern Taiwan. *Geophys. Res. Lett.*, 32, L10313. doi:10.1029/2005GL022861.

Lin, C. H. (2016), Evidence for a magma reservoir beneath the Taipei metropolis of Taiwan from both S-wave shadows and P-wave delays. *Scientif. Rep.*, 6, 39500.

Lin, C. H. (2017a), Probable dynamic triggering of phreatic eruption at the Tatun volcano group of Taiwan. *J. Asian Earth Sci.*, 149, 78–85.

Lin, C. H. (2017b), Dynamic triggering of drumbeat seismicity at Tatun volcano group in Taiwan. *Geophys. J. Int.*, 210, 354–359.

Lin, C. H., Lai, Y. C., Shih, M. H., Pu, H. C., & Lee, S. J. (2018), Seismic detection of a magma reservoir beneath Turtle Island of Taiwan by S-wave shadows and reflections. *Scientif. Rep.*, 8, 16401.

Liu, T. K., Hsieh, S., Chen, Y. G., & Chen, W. S. (2001), Thermo-Kinematic evolution of the Taiwan oblique-collision mountain belt as revealed by zircon fission track dating. *Earth Planet. Sci. Lett.*, 186, 45–56.

McVey, B. G., Hooft, E. E. E., Heath, B. A., Toomey, D. R., Paulatto, M., Morgan, J. V., Nomikou, P., & Papazachos, C. B. (2019), Magma accumulation beneath Santorini volcano, Greece, from P-wave tomography. *Geology*, https://doi.org/10.1130/G47127.1

Nur, A., Mavko, G., Dvorkin, J., & Galmudi, D. (1998), Critical porosity: a key to relating physical properties to porosity in rocks. *Lead. Edge*, 17, 357–362.

Rawlinson, N., & B. L. N. Kennett (2004), Rapid estimation of relative and absolute delay times across a network by adaptive stacking. *Geophys. J. Int.*, 157, 332–340.

Shin, T.C. (1992), Some implications of Taiwan tectonic features from the data collected by the Central Weather Bureau Seismic Network. *Meteorol. Bull.*, 38, 23–48 (in Chinese).

Shin, T. C., Tsai, Y. B., Yeh, Y. T., Liu, C. C., & Wu, Y. M. (2003), Strong motion instrumentation programs in Taiwan, In:Lee, W. H. K., Kanamori, H., Jennings, P. C. (Eds.), Handbook of Earthquake and Engineering Seismology, Academic Press, New York, pp.1057–1602.

Song, S.-R., Yang, T.-F., Yeh, Y.-H., Tsao, S.-J., & Lo, H.-J. (2000), The Tatun volcano group is active or extinct? *J. Geol. Soc. China*, 43, 521–534.

Suppe, J. (1984), Kinematics of arc–continent collision, flipping of subduction, and back-arc spreading near Taiwan. *Mem. Geol. Soc. China*, 6, 21–33.

Teng, L. S. (1996), Extensional collapse of the northern Taiwan mountain belt. *Geology*, 24, 949-952.

Teng, L. S., Lee, C. T., Tsai, Y. B., & Hsiao, L. Y. (2000), Slab breakoff as a mechanism for flipping of subduction polarity in Taiwan. *Geology*, 28, 155–158.

Toomey, D. R., & Foulger, G. R. (1989), Tomographic inversion of local earthquake data from the Hengill-Grensdalur central volcano complex, Iceland. *J. Geophys. Res.*, 94, 17,497–17,510. doi:10.1029/JB094iB12p17497.

Tsao, S. J. (1994), Potassium-argon age determination of volcanic rocks from the Tatun volcano group. *Bulletin of the Central Geological Survey*, 9, 137-154 (in Chinese).

Um, J., & Thurber, C. (1987), A fast algorithm for two-point seismic ray tracing. *Bull. Seismol. Soc. Am.*, 77, 972–986.

Ustaszewski, K., Wu, Y.-M., Suppe, J., Huang, H.-H., Chang, C.-H., & Carena, S. (2012), Crust-mantle boundaries in the Taiwan - Luzon arc-continent collision system determined from local earthquake tomography and 1D models: Implications for the mode of subduction polarity reversal. *Tectonophysics*, 578, 31-49.

Wang, W.-S., & Chen, C.-H. (1990), The volcanology and fission track age dating of pyroclastic deposits in Tatun Volcano group, northern Taiwan. *Acta Geologica Taiwanica*, 28, 1-30.

Wang, K.-L., Chung, S.-L., Chen, C.-H., Shinjo, R., Yang, T.-F., & Chen, C.-H. (1999), Post-collisional magmatism around northern Taiwan and its relation with opening of the Okinawa trough. *Tectonophysics*, 308, 363–376.

Wang, K.-L., Chung, S.-L., O'Reilly, S. Y., Sun, S.-S., Shinjo, R., & Chen, C.-H. (2004), Geochemical constraints for the genesis of post-collisional magmatismand the geodynamic evolution of the Northern Taiwan Region. *Journal of Petrology*, 45, 975–1011.

Wang, H.-L., Zhu, L., & Chen, H.-W. (2010), Moho depth variation in Taiwan from teleseismic receiver functions. *Journal of Asian Earth Sciences*, 37, 286–291.

Wu, Y.-M., Chang, C.-H., Zhao, L., Shyu, J.B.H., Chen, Y.-G., Sieh, K., & Avouac, J.-P. (2007), Seismic tomography of Taiwan: improved constraints from a dense network of strong motion stations. *J. Geophys. Res.*, 112, B08312. doi:10.1029/2007JB004983.

Wu, Y.-M., Shyu, J.B.H., Chang, C.-H., Zhao, L., Nakamura, M., & Hsu, S.-K. (2009), Improved seismic tomography offshore northeastern Taiwan: implications for subduction and collision processes between Taiwan and the southernmost Ryukyu. *Geophys. J. Int.*, 178, 1042–1054.

Yang, T. F., Sano, Y., & Song, R. S. (1999), $^{3}He/^{4}He$ ratios of fumaroles and bubbling gases of hot springs in Tatun volcano group, north Taiwan. *Nuovo Cim.*, 22, 281–285.

Zelt, C.A. (1998), Lateral velocity resolution from three-dimensional seismic refraction data. *Geophys. J. Int.*, 135, 1101–1112.

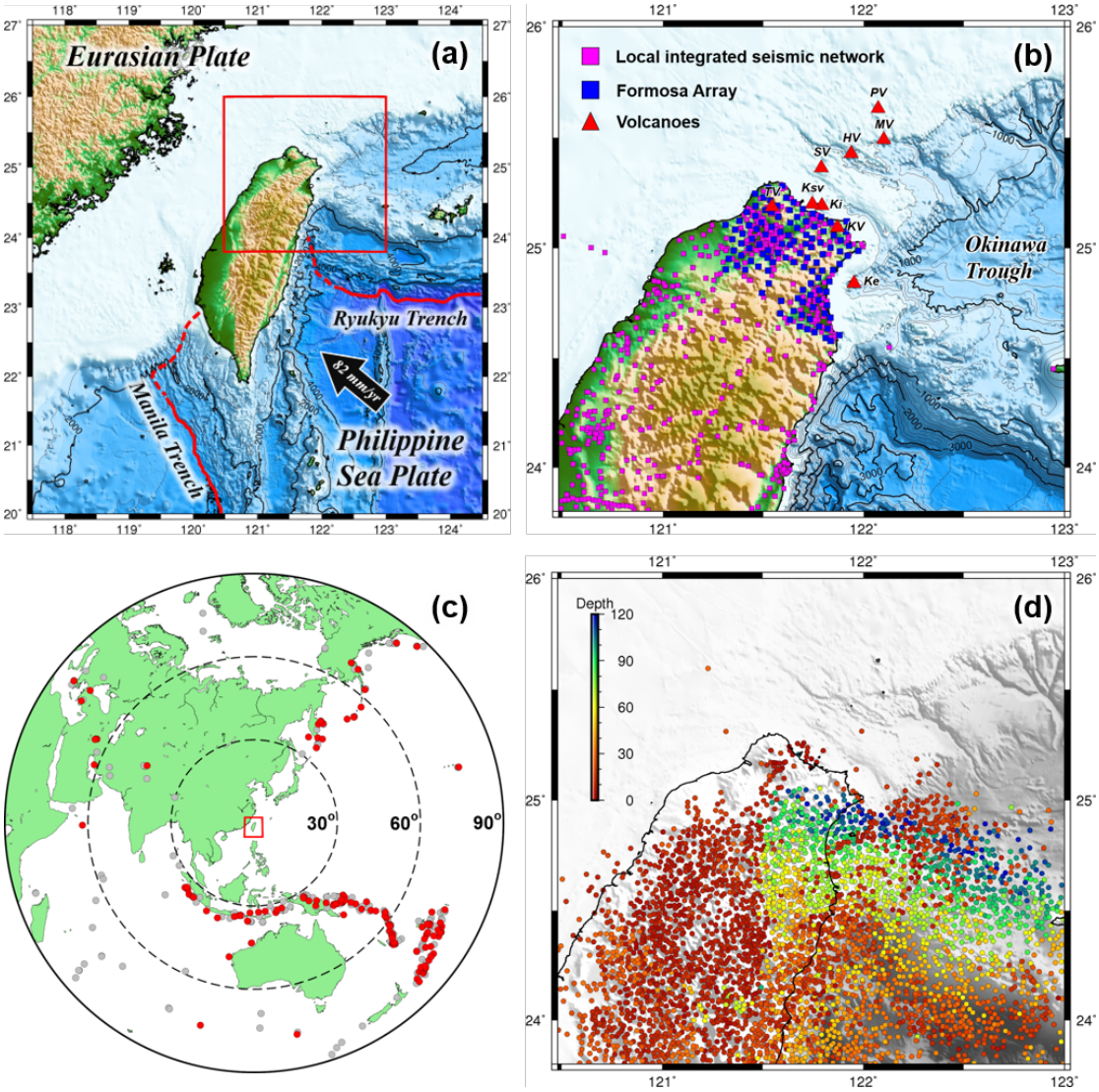

Figure 1. Tectonic and data distribution maps. (a) Tectonic setting of the Taiwan region where the Philippine Sea plate subducts northward along the Ryukyu trench and the Eurasian plate subducts eastward along the Manila trench. The black arrow shows the plate motion at 82 mm/yr. The red box shows the study area. (b) Distribution of stations used and regional volcanoes. Purple and blue squares denote the stations of local integrated seismic network and Formosa Array. Red triangles indicate the volcanoes. (c) Distribution of teleseismic events recorded (gray dots) and used (red dots). (d) Distribution of local earthquakes, color coded by focal depth.

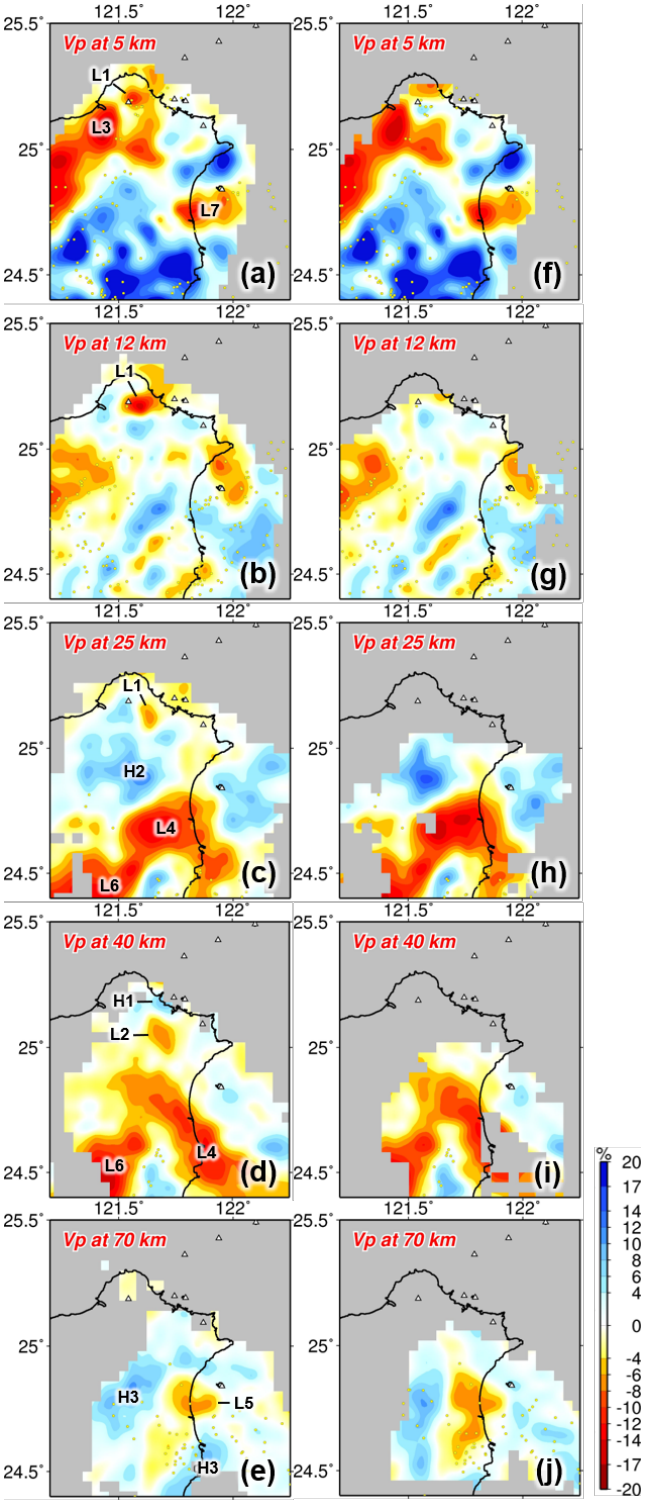

Figure 2. Model results at different depths (a-d) with and (e-h) without Formosa Array teleseismic data. Warm and cold colors represent the low and high P-wave velocities. Labels indicate the velocity anomalies discussed in the text.

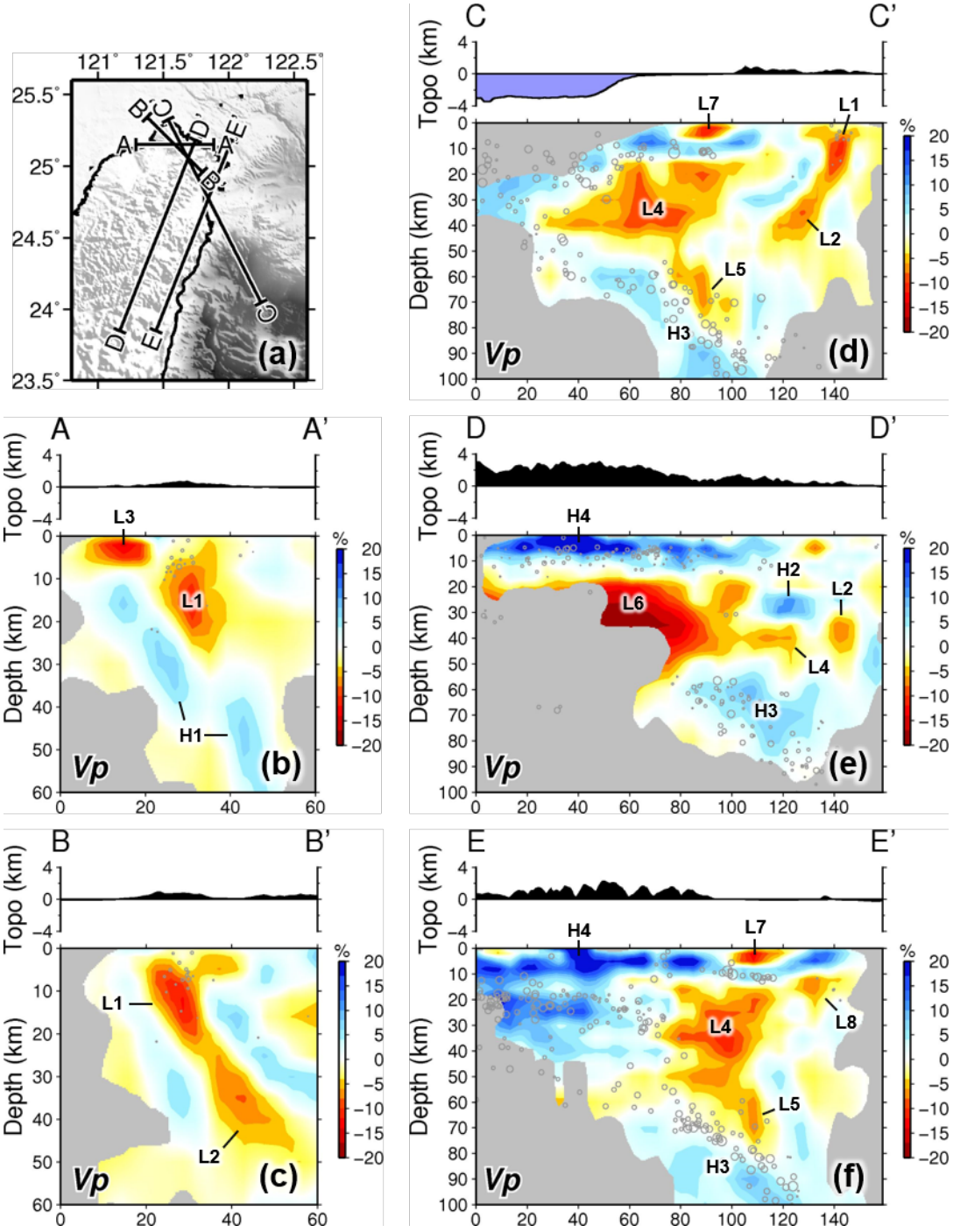

Figure 3. Model results in different cross sections. (a) Locations of cross sections AA'-EE' shown in (b-f). Warm and cold colors represent the low and high P-wave velocities. Labels indicate the velocity anomalies discussed in the text.

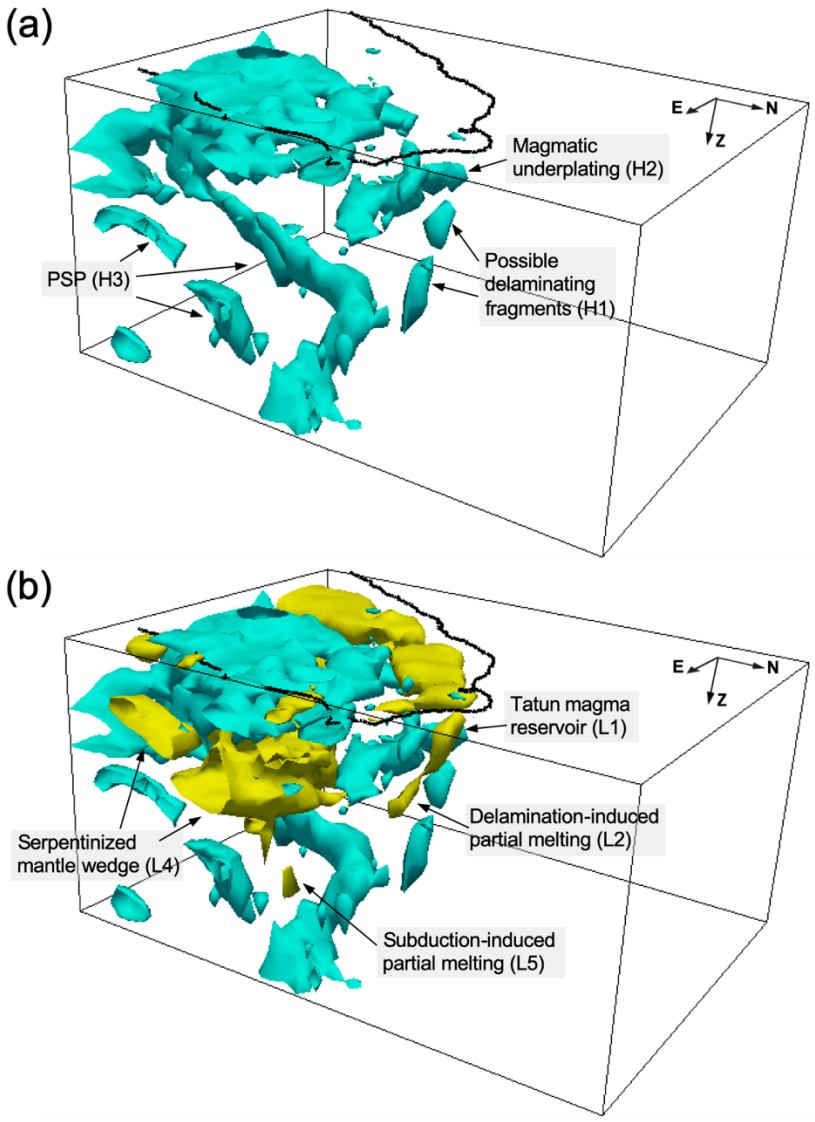

Figure 4. 3-D perspective and interpretations of 3-D velocity structures in the northern Taiwan. Yellowish and cyanish bodies represent the low and high velocity anomalies with magnitude greater than ±6%.